SUPPLEMENTARY INFORMATION

2p or not 2p: Tuppence-based SERS for the detection of illicit materials

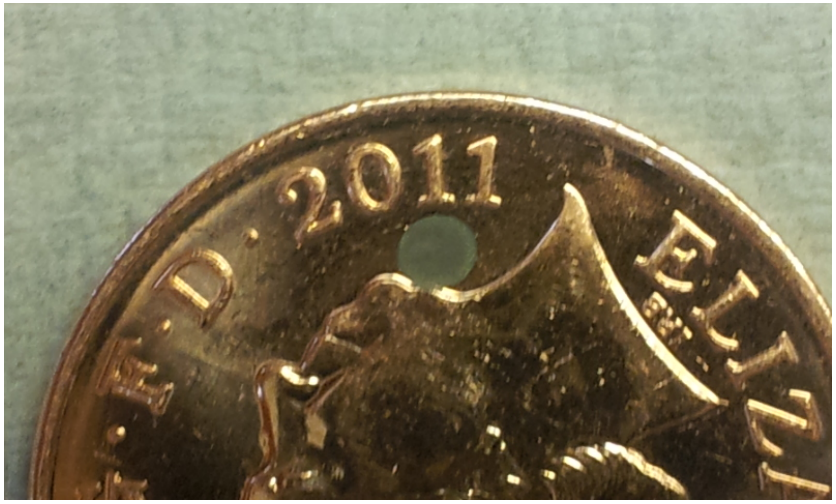

Figure S1. Deposition of silver (Grey target) demonstrated on a post-1992 2p coin.

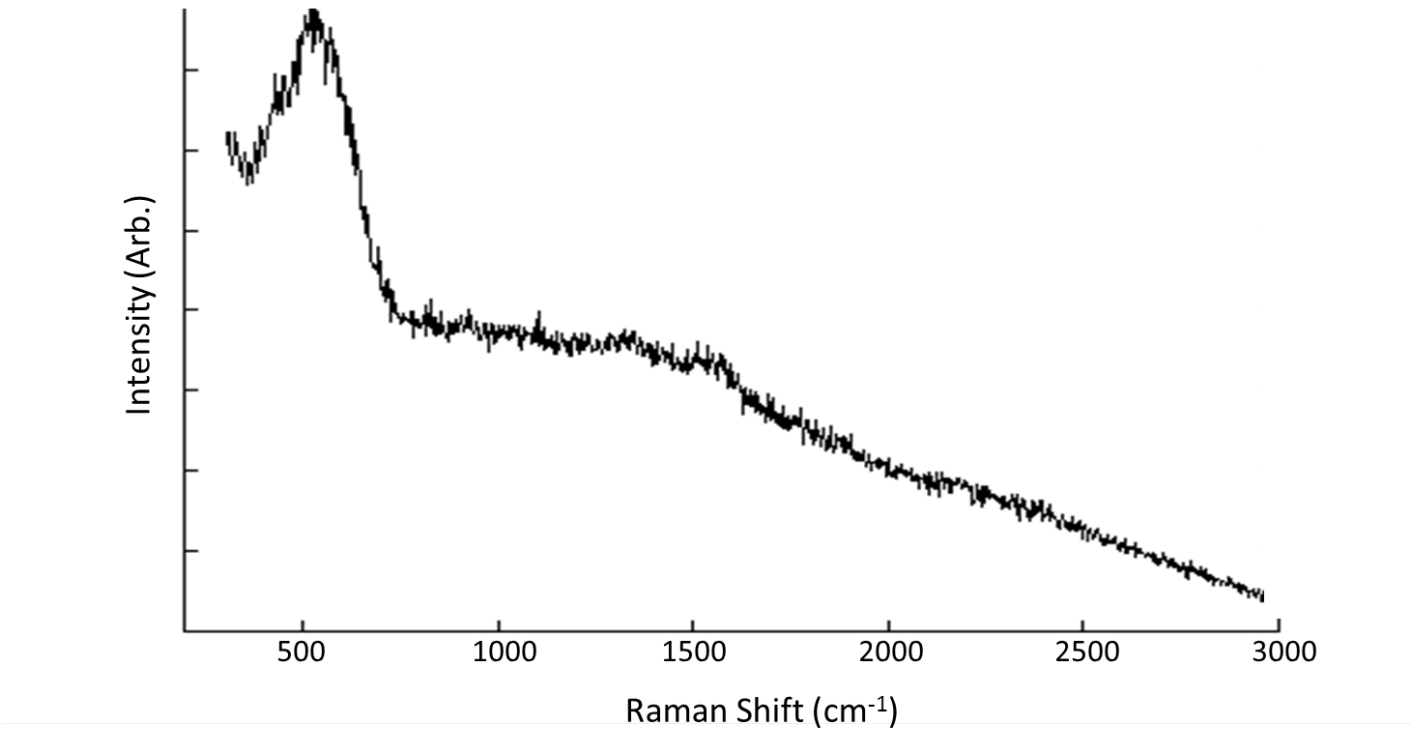

Figure S2. Raman spectrum generated when Mephedrone ($1x10^{-4}$M) was spotted onto the bare copper coin.

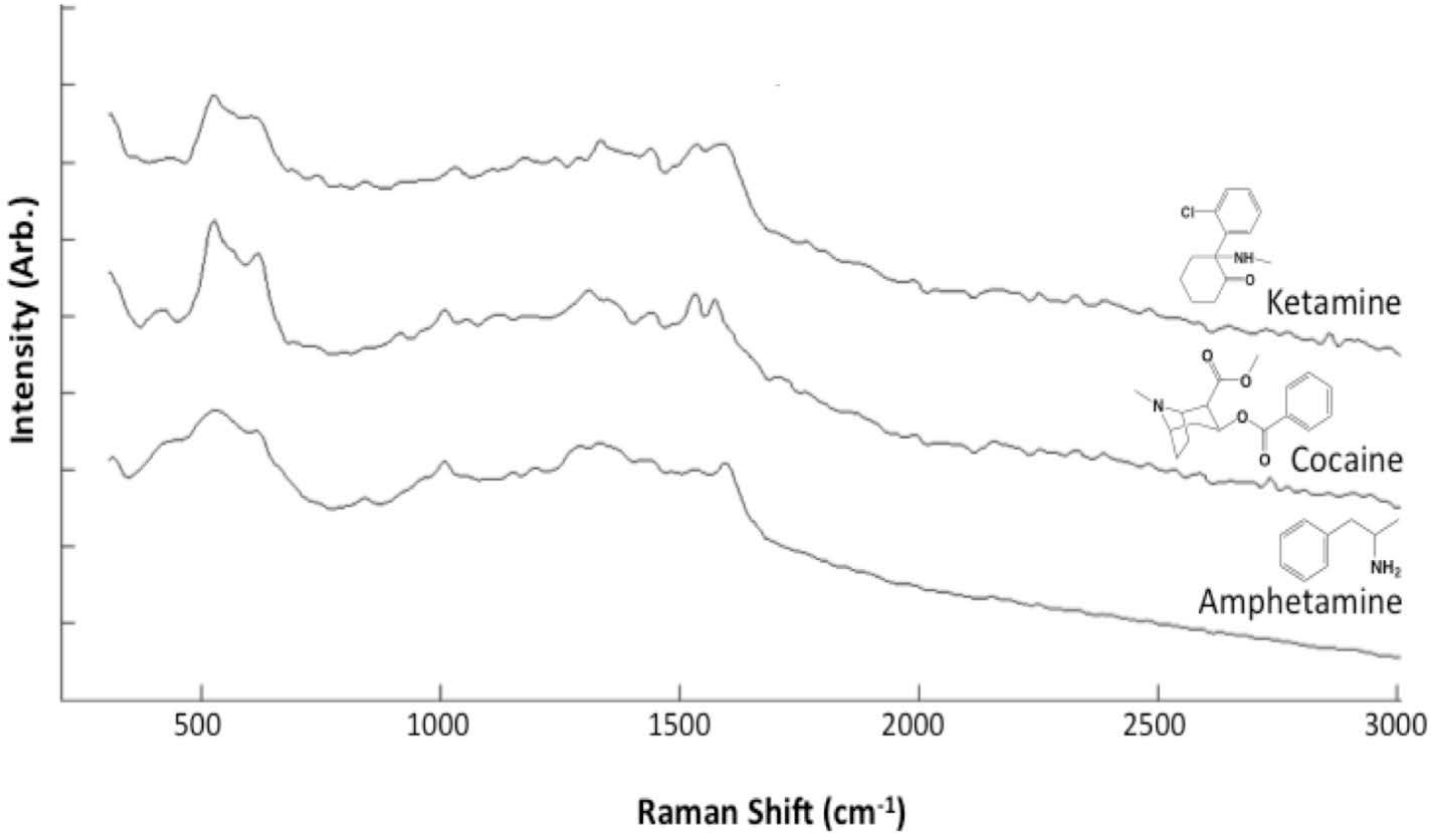

Figure S3. Representative SERS spectra of the drugs ketamine, cocaine and amphetamine acquired from the silver surface.

All vibrational assignments were carried out using: G. Socrates*. Infrared and Raman Characteristic Group Frequencies: Tables and Charts*, Wiley: New York, U.S.A. 2001.

Table S1. Tentative SERS vibrational assignments for Mephedrone

Raman Shift (cm^{-1})	**Vibration Assignment**
418.6	CNC def
530	CCC ring or CO deformation
602.2	In plane ring deformation
698.5	Asym CNC stretch or ring vib para substituted benzene
741.5	Asym CNC stretch or ring vib para substituted benzene
799.5	C-H out-of-plane bending vibration
899	Unassigned
991.3	Unassigned
1030	CH in plane deformation (benzene)
1103	Sym CNC str
1215	CN Stretch or para disubstituted ring vibration
1292	Unassigned
1354	CH_3CO- (Symmetrical CH_3 deformation)
1459	Unassigned
1509	NH deformation secondary Amine
1558	Benzene derivative C=C str
1604	Benzene derivative C=C str or C=C conjugated with C=O
1657	C=O stretch

Table S2. Tentative SERS vibrational assignments for MDMA

Raman Shift (cm^{-1})	Vibrational Assignment
315.2	Unassigned
425	Unassigned
466.5	Unassigned
517.3	CCC ring
567.8	CCC ring
617.8	CCC ring
729.2	Unassigned
814.6	OCCO
860	CNC
967.6	COC
1050	Unassigned
1108	CH_2
1149	CNC
1201	Unassigned
1246	CH
1337	Unassigned
1429	CH_3/CH_2 scissors
1465	CH_3/CH_2 scissors
1514	COC
1558	Unassigned

Table S3. Tentative SERS vibrational assignments for MDAI

Raman Shift (cm^{-1})	**Vibrational Assignment**
453.8	Tetrasubstituted Benzene
472.9	Tetrasubstituted Benzene
514.2	Tetrasubstituted Benzene
611.6	Tetrasubstituted Benzene
744.6	Unassigned
814.6	sym C-O-C str
863	C-H out of plane deformation associated with benzene ring
917	Unassigned
961.6	cyclo pentene ring vibration
1033	1,3-dioxolane ring vibration
1103	primary amine vibration or 1,3 dioxolane ring vibration
1212	Unassigned
1337	Unassigned
1370	C=C str (dioxolane)
1476	1,2,4,5-tetrasubstituted benzene vib
1530	1,2,4,5-tetrasubstituted benzene vib
1569	Unassigned
1700	Unassigned

Table S4. Tentative SERS vibrational assignments for Ketamine

Raman Shift (cm^{-1})	Vibrational Assignment
360.6	C-Cl stretch
434.6	CNC def, C-Cl stretch
526.8	C-Cl stretch
611.6	Unassigned
692.3	orthosubstituted benzene
741.5	orthosubstituted benzene
790.3	Unassigned
841.9	Unassigned
922.9	Unassigned
1030	orthosubstituted benzene
1076	orthosubstituted benzene
1108	Unassigned
1178	orthosubstituted benzene
1238	Unassigned
1286	Unassigned
1337	Unassigned
1440	orthosubstituted benzene
1533	orthosubstituted benzene
1590	orthosubstituted benzene
1763	possible ketone str

Table S5. Tentative SERS vibrational assignment for Cocaine

Raman Shift (cm^{-1})	Vibrational Assignment
418.6	Aromatic Ring
526.8	Unassigned
617.8	Aromatic ring
695.4	Unassigned
735.4	Unassigned
793.4	Piperidine ring
847.9	Unassigned
914	Unassigned
1009	Benzoic acid
1053	Benzoic acid
1126	Unassigned
1178	Unassigned
1309	Unassigned
1351	Unassigned
1443	Cyclic CH_2/CH_3
1489	Unassigned
1530	Unassigned
1571	Aromatic ring or benzyl ring
1708	Unassigned
1768	Unassigned
1857	Unassigned

Table S6. Tentative SERS vibrational assignments for Amphetamine

Raman Shift (cm^{-1})	Vibrational Assignment
428.2	$(SO_4)^{2-}$ asym stretch
530	Unassigned
614.7	Aromatic ring bend
738.4	Aryl C-H wag
838.9	Alkyl c-c
967.6	$(SO_4)^{2-}$ asym stretch
1009	monosubstituted aromatic ring breathing mode
1053	CC aromatic ring vibration
1103	Unassigned
1149	Unassigned
1195	C-N
1289	Unassigned
1337	Unassigned
1432	Unassigned
1484	Unassigned
1530	Unassigned
1596	CCH aromatic ring stretch

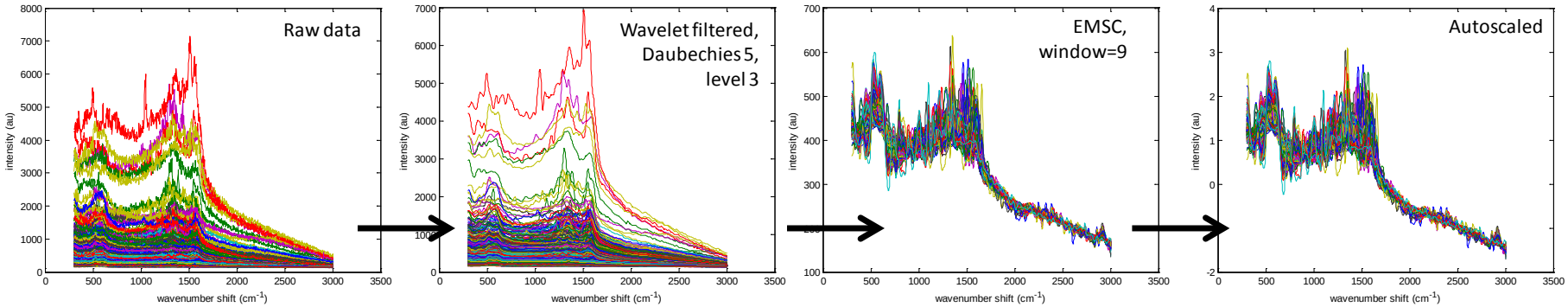

Figure S4. Data pre-processing of the SERS spectra. The processing is detailed below:

1. Plots of the 249 Raw Raman spectra analysed.
2. The raw Raman spectra were filtered by using Daubechies 5 wavelet function with 3 levels of decomposition. The detail coefficients were replaced with 0s while the approximation coefficients were kept the same. The Raman spectra were then reconstructed by using the wavelet coefficients to remove the high frequency noises and spikes (S. Mallat (1989) *IEEE Pattern Analysis and Machine Intelligence* **11**, 674-693).
3. The data were next normalised using extended multiplicative scatter correction using a bin size of 9 (H. Martens *et al. Anal. Chem*., 2003, 75, 394-404).
4. Finally these data were then autoscaled. This is a form of scaling which mean-centres each value of the column followed by dividing row entries of a column by the standard deviation within that column (R. Goodacre *et al*. (2007) *Metabolomics* **3**, 231-241).

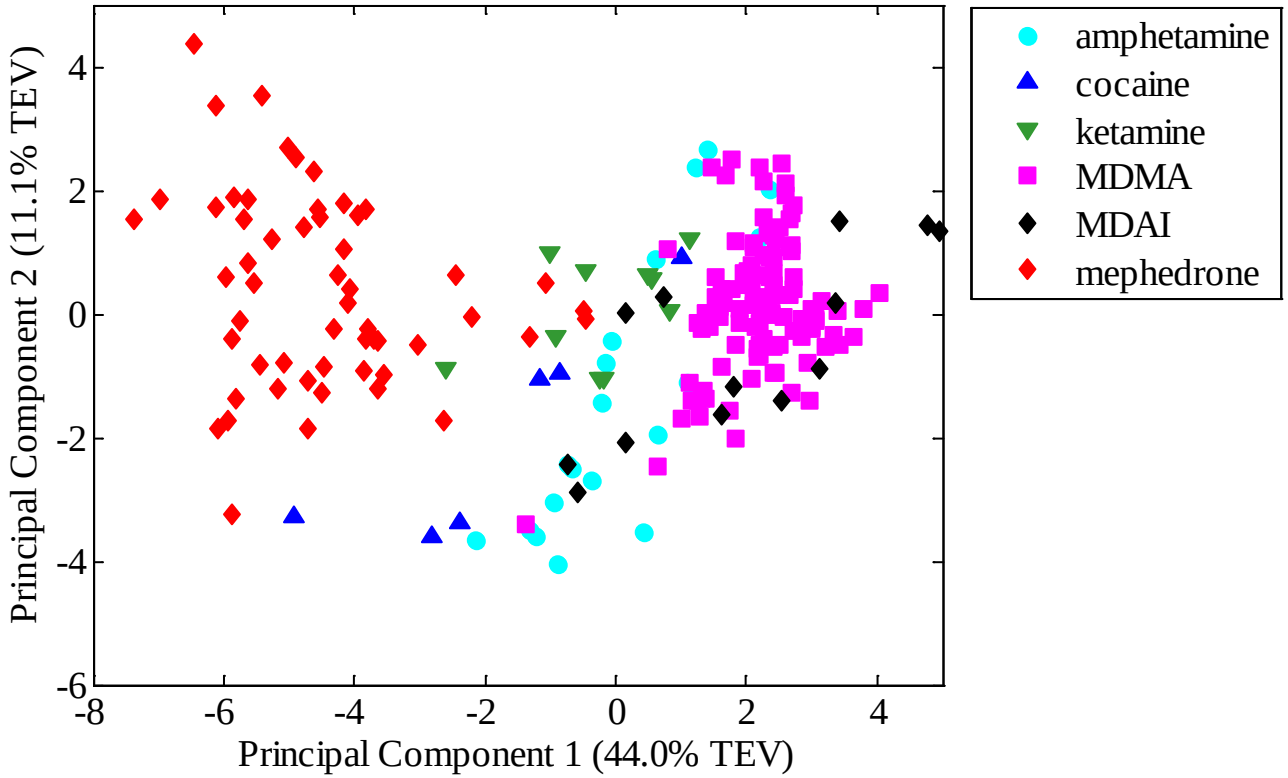

Figure S5. Principal components analysis (PCA) scores plot of the processed SERS spectra. In general the replicate spectra are located near one another highlighting the excellent spectral similarity. Details of PCA can be found in (R. Goodacre *et al*. (1998) *Microbiology* **144**, 1157-1170).

PLS predictions of drugs:

The full set of results from bootstrapped PLS1 calibration (1000 iterations) for the three drugs: MDMA, MDAI and Mephedrone. For each figure (Figures S4A-C) there are four components that are labelled as:

A. Boxplot depicting the mean training and test predictions for each sample across all 1000 bootstrapped models.. The boxes have lines at the lower quartile, median, and upper quartile values; the whiskers are lines extending from each end of the boxes to show the extent of the rest of the data, and outliers are marked by crosses.
B. Histogram showing the distribution of training and test predictions across all 1000 bootstrapped models.
C. Receiver operating characteristic (ROC) & ROC convex hull (ROCCH) give the true-positive (TP) rate and false positive (FP) rate of classification; ROC curves are beneficial because they avoid having to apply a numerical threshold which defines the class boundary. A ROC curve with an area of 1 shows 100% classification accuracy. For this study the ROC has been calculated using the full complement of test predictions only across all 1000 bootstrapped models.
D. A confusion matrix giving the number of true positive (TP), false positive (FP), true negative (TN), false negative (FN) classifications based upon the mean of PLS1 test predictions for each sample across the 200 bootstrapped models. This is based upon an arbitrary classification boundary of >=0.5 (positive), <0.5 (negative). Some common metrics that can be derived from this calculation (sensitivity, specificity, precision and accuracy) are also provided. Where:

$$sensitivity = \frac{TP}{TP + FN} \qquad specificity = \frac{TN}{TN + FP}$$

$$precision = \frac{TP}{TP + FP} \qquad accuracy = \frac{TP + TN}{TP + FP + TN + FN}$$

The above process was adapted from (K. Faulds *et al*. (2008) *Analyst* **133**, 1505-1512).

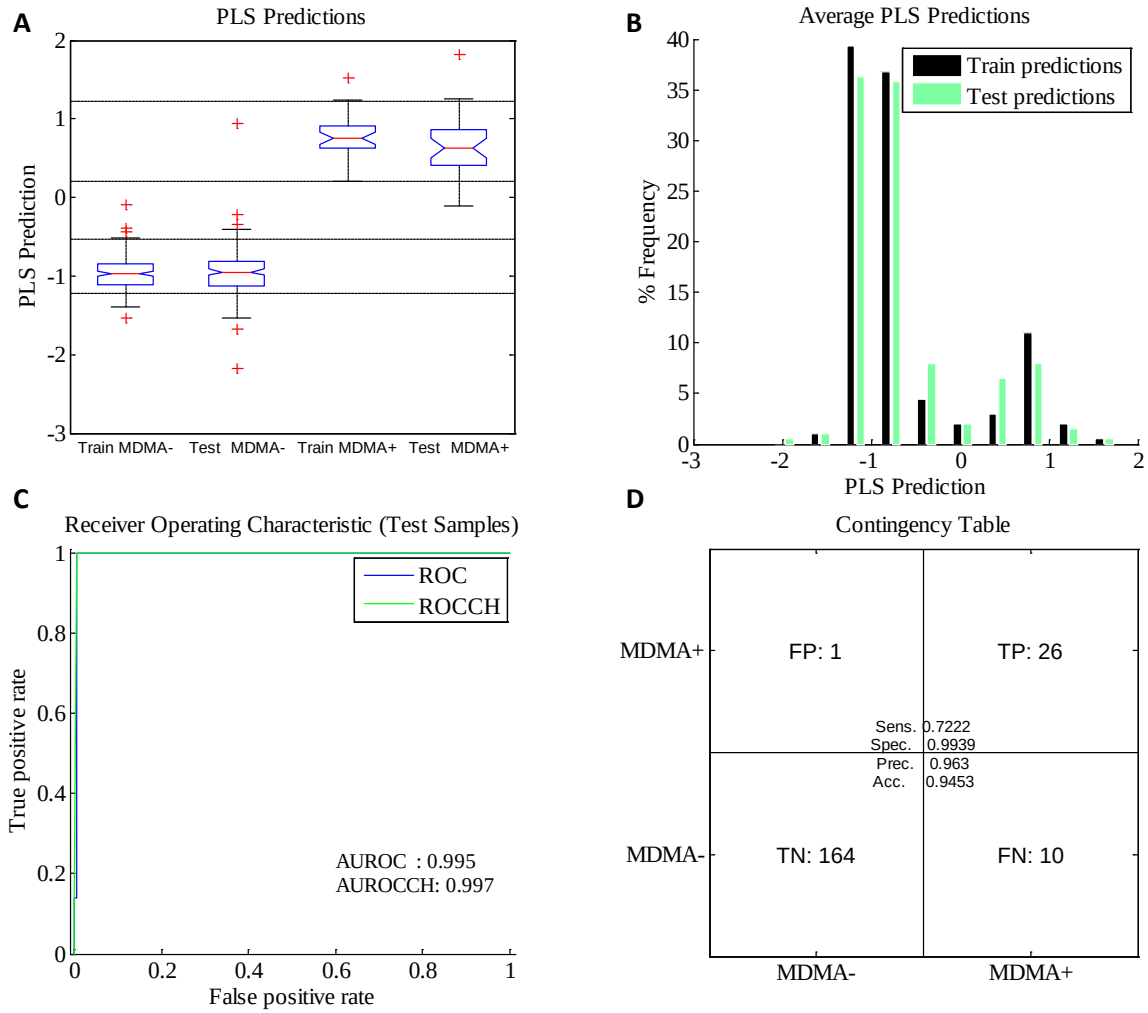

Figure S6A. PLS1 bootstrap results for MDMA

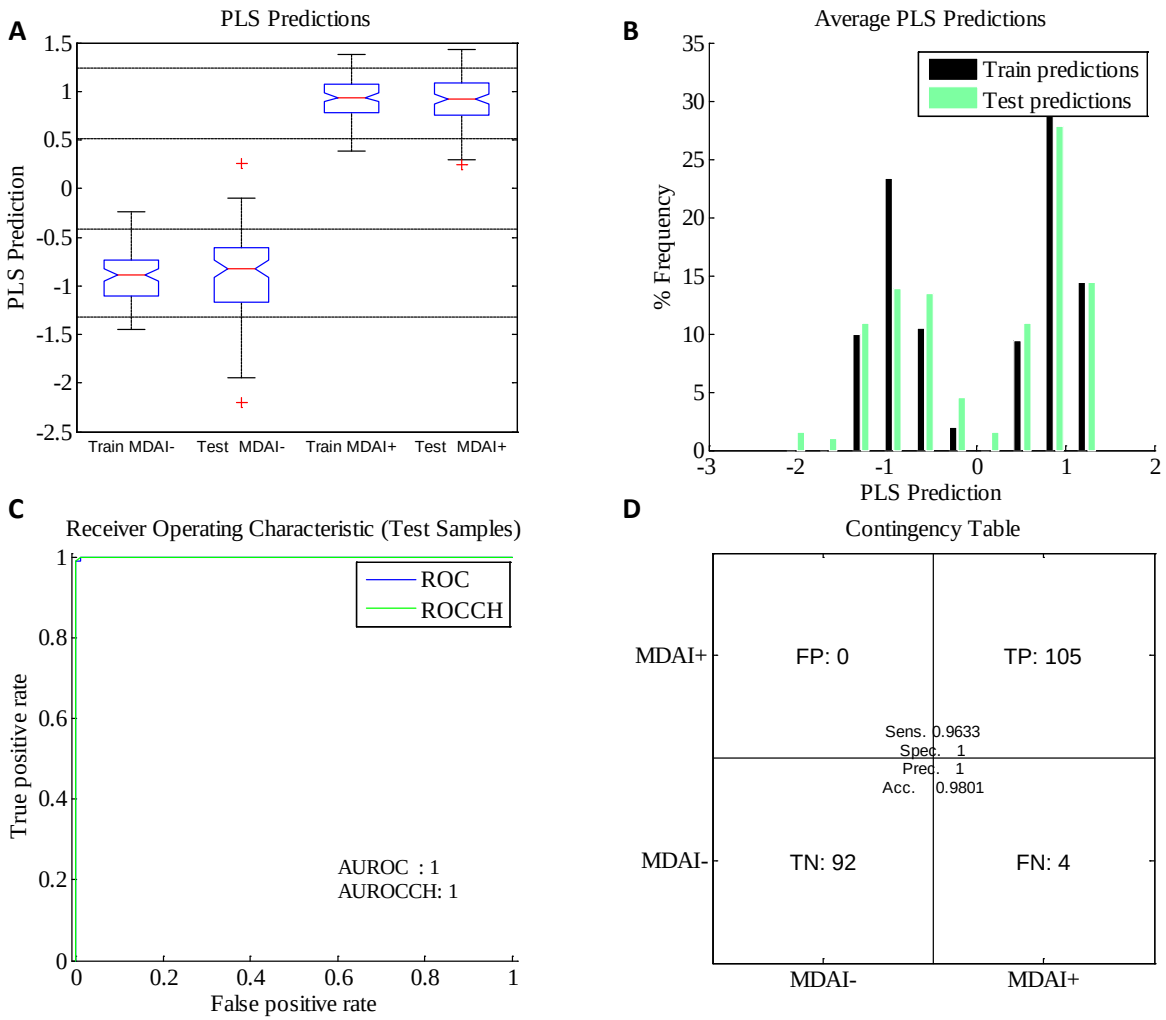

Figure S6B. PLS1 bootstrap results for MDAI.

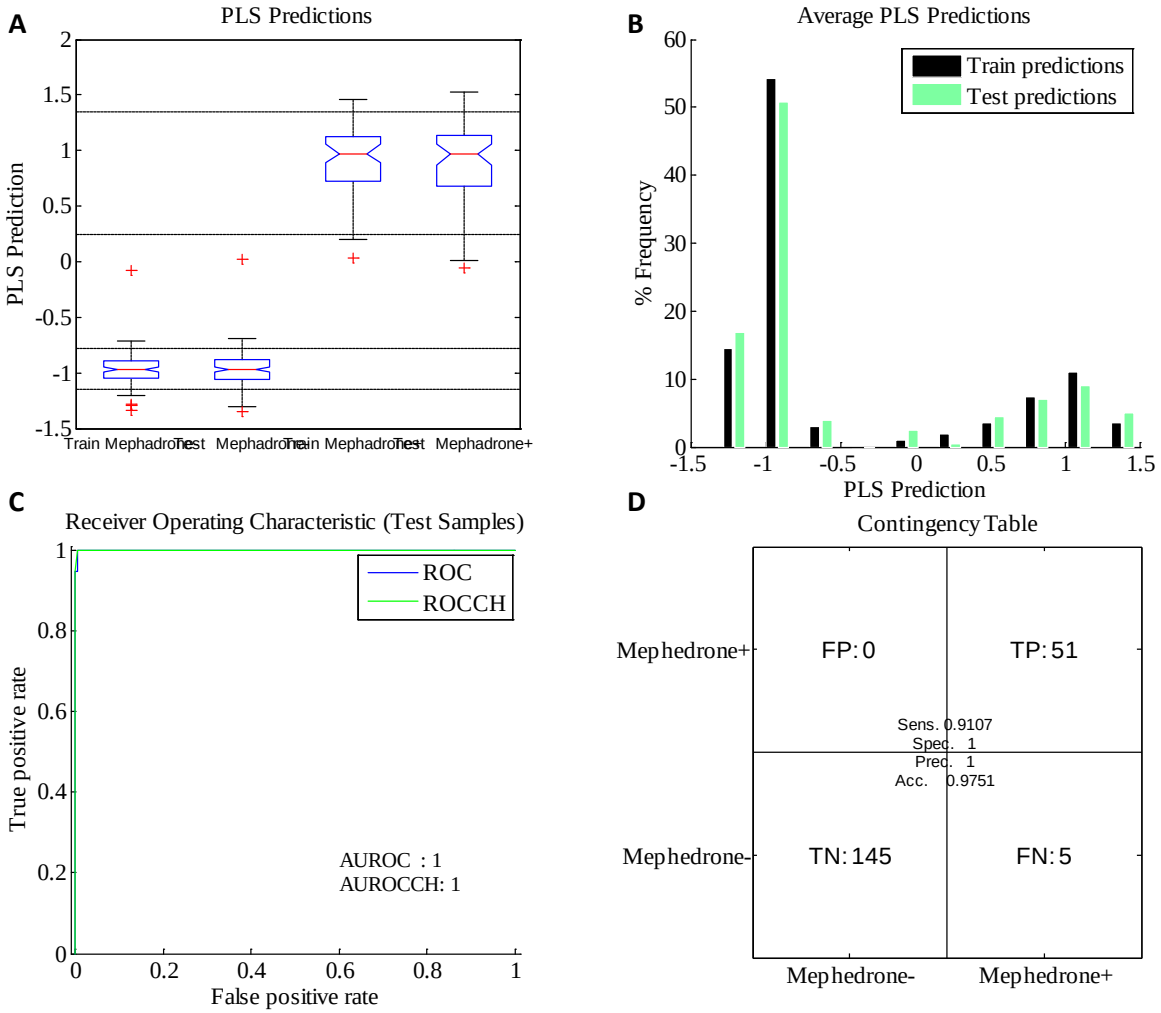

Figure S6C. PLS1 bootstrap results for Mephedrone

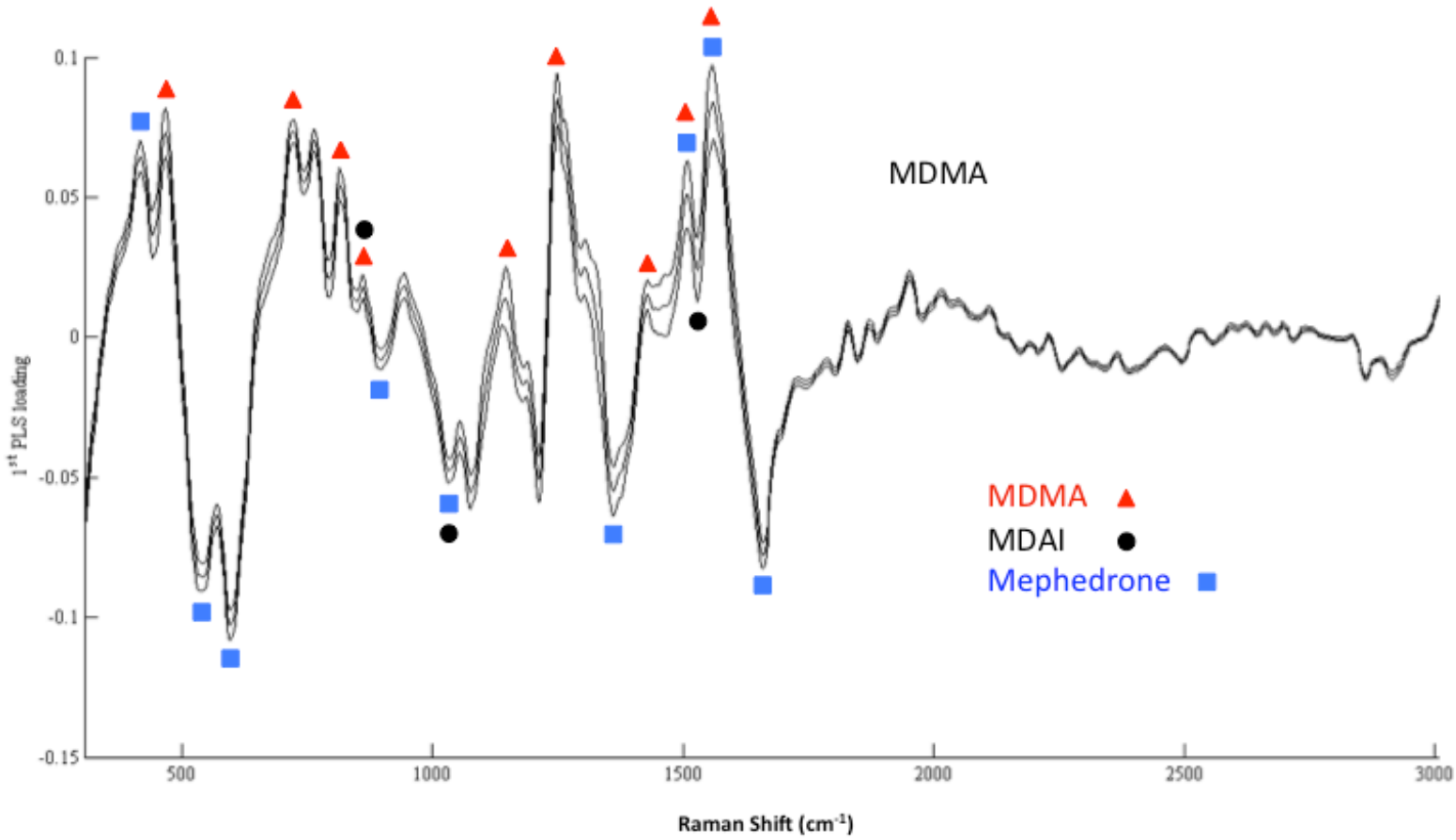

Figure S7A. Annotated PLS1 Loadings Plots for MDMA. The red triangles represent vibrations from MDMA, black circles represent vibrations from MDAI and blue squares represent vibrations from Mephedrone.

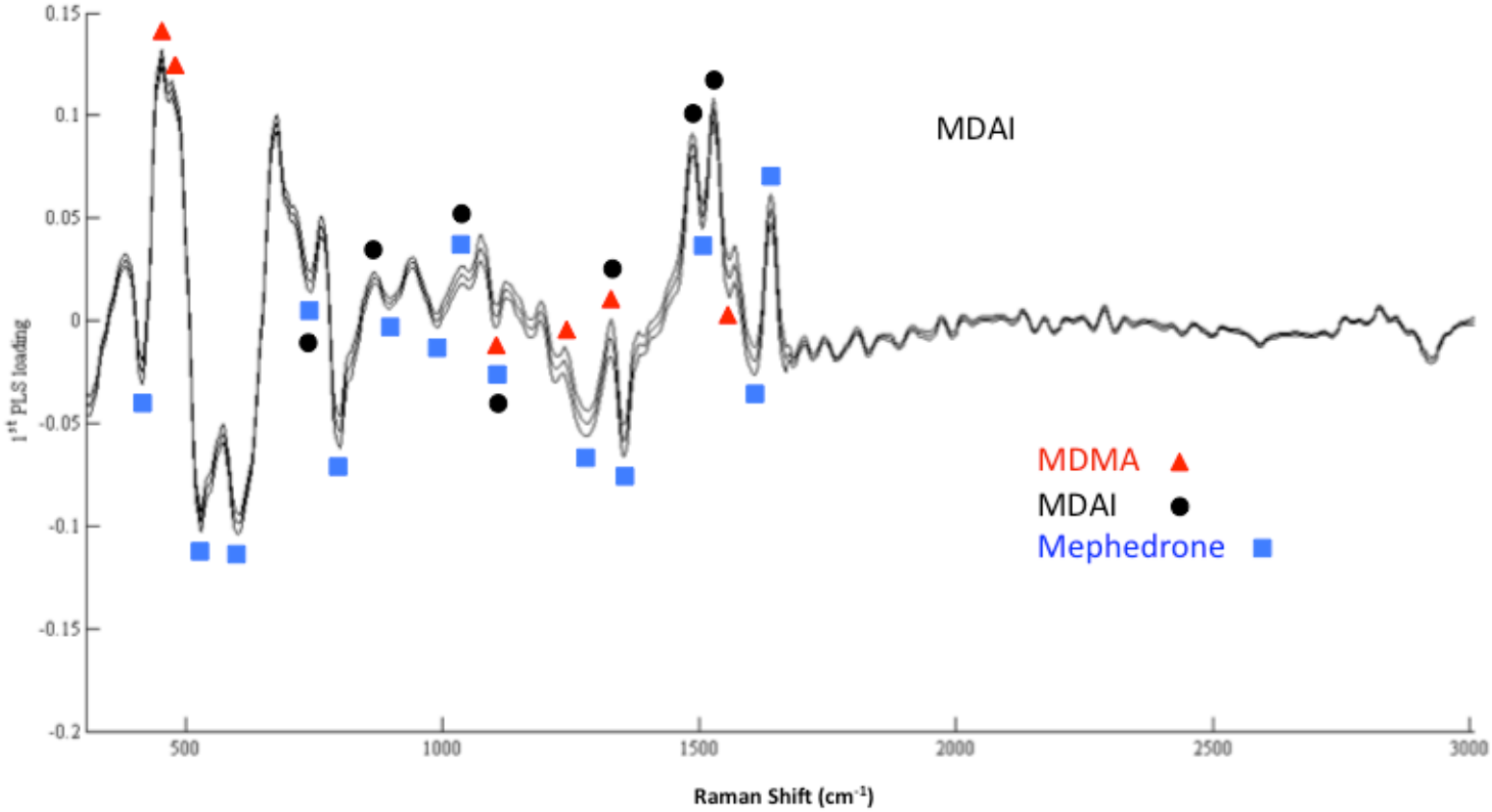

Figure S7B. Annotated PLS1 Loadings Plots for MDAI. The red triangles represent vibrations from MDMA, black circles represent vibrations from MDAI and blue squares represent vibrations from Mephedrone.

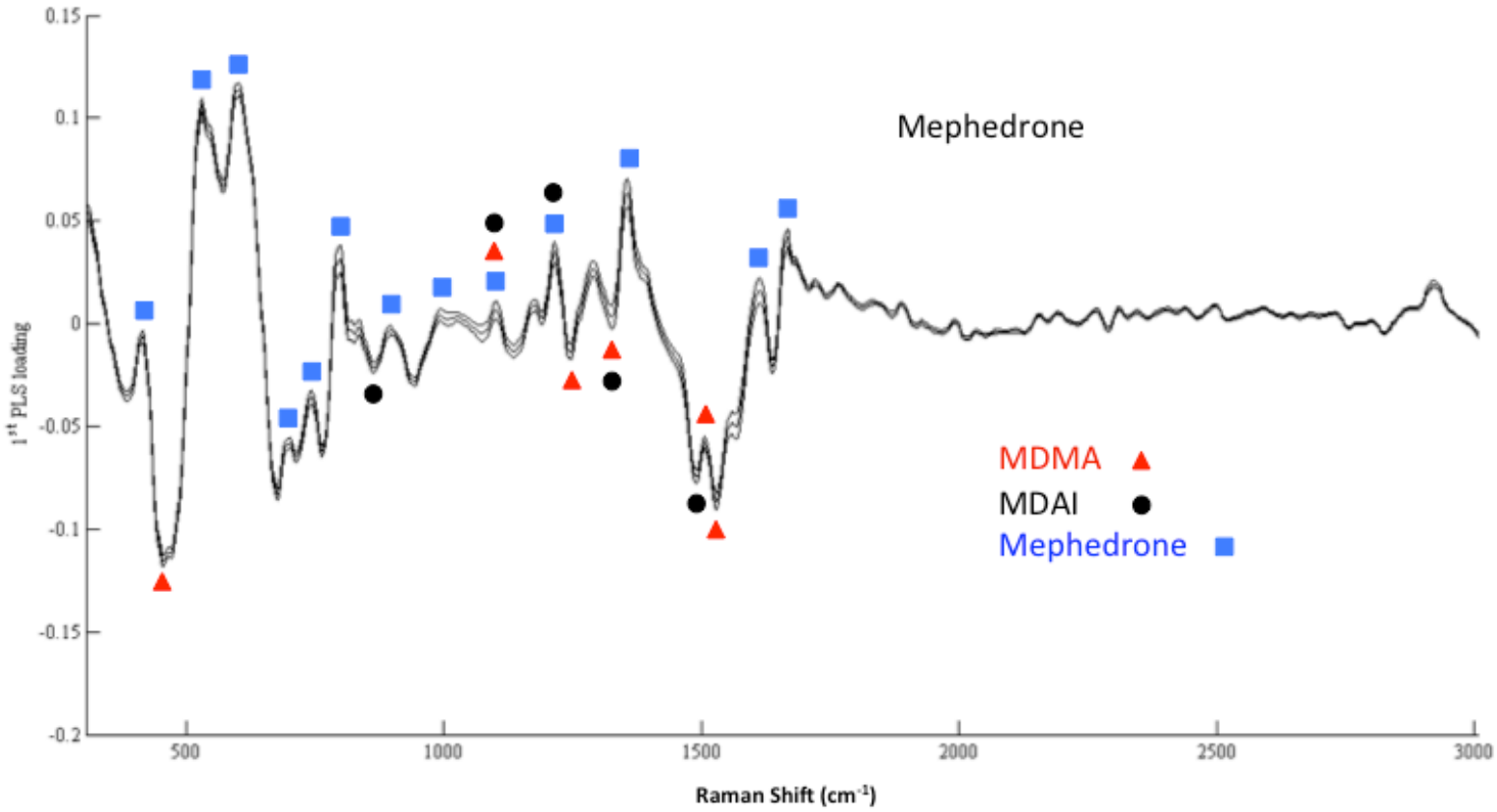

Figure S7C. Annotated PLS1 Loadings Plots for Mephedrone. The red triangles represent vibrations from MDMA, black circles represent vibrations from MDAI and blue squares represent vibrations from Mephedrone.